ISSN 0016-8521, Geotectonics, 2022, Vol. 56, No. 2, pp. 107–122. © The Author(s), 2022. This article is an open access publication.
Russian Text © The Author(s), 2022, published in Geotektonika, 2022, No. 2, pp. 3–20.

Relationships of Surface Geological and Geophysical Characteristics with the Deep Structure of the Mid-Atlantic Ridge According to Seismic Tomography Data

S. Yu. Sokolov[a], *, K. O. Dobrolyubova[a], and N. N. Turko[a]

[a] *Geological Institute, Russian Academy of Sciences (GIN RAS), Moscow, 119017 Russia*

**e-mail: sysokolov@yandex.ru*

Received August 6, 2021; revised February 11, 2022; accepted February 28, 2022

Abstract—A retrospective analysis of seismic tomography models with different levels of detail along the Mid-Atlantic Ridge (MAR) has shown that mantle inhomogeneities depicted by variations of seismic waves velocities in low-detail models look larger than their true sizes determined by more detailed modern models. They also confirm that there are two different types of upwelling in the Atlantic mantle: active plume, which has an impulsive character, and passive axial, which occurs as a response to spatial appearance during the drift of lithospheric plates. The structure of mantle velocity and density inhomogeneities, determined by low-frequency gravity anomalies and their reductions, has a consistent interpretation based on the thermal state of the mantle. Detailed models of the velocities under the MAR can serve as a basis for comparison with the geochemical characteristics of basalts. The decomposition of a single axial tomographic anomaly in detailed models into a chain of vertical lenses under slow spreading conditions corresponds to geochemical data on discrete manifestations of different basalt associations along the MAR. The attribute $\delta(V_p/V_s)$ section along the MAR in the mantle above ~700 km contains cold lenses with a thickness of 200–300 km, which are spatially related to the following structural and tectonic phenomena: transform faults with maximum lateral rift displacement; geochemical segmentation of the MAR; modulation of the total lengths of transform faults with increased values above the "cold" lenses; asymmetry features of the half-spreading rates, which decreases to zero above the cold lenses and reaches maximum values between the cold lenses. The cold mantle lenses at an average depth of ~500 km and the corresponding lithospheric geophysical characteristics reflect the background conditions, and areas above hot segments are disturbances that occur when plume branches interfere with the MAR. Inhomogeneous spreading rates can lead to movements of blocks inside large plates and tectonic deformations of the intraplate space. Along the 4 Ma isochron in the Northern Hemisphere, the half-spreading rates on the eastern flank of the MAR exceed the half-spreading rates on the western flank. In the Southern Hemisphere, the pattern is reversed, which indicates the possible influence of the Earth's rotation effects on geodynamic processes along the MAR. Against the general trend, there are local inversion zones from the western predominance of increased rates to the eastern and, conversely, in the Northern and Southern hemispheres. The main demarcation faults of the Atlantic differ in seismic events by their maximum energy release and are located near the "cold" mantle lenses and the contrasting lateral transition to the hot regions. The distribution of the total seismic moment in the depth intervals of 0–13 and 13–35 km also has less intense extremes near the branches of plumes with a predominantly crustal position of the hypocenters. The seismicity along the main MAR space associated with standard basalt magmatism has a background character and does not significantly contribute to the total released seismic moment compared to shear zones.

Keywords: seismic tomography, geological-geophysical data, seismicity, Mid-Atlantic Ridge (MAR), mantle inhomogeneities, topography, gravity, basalts, transform faults, geology, tectonics

DOI: 10.1134/S0016852122020066

INTRODUCTION

The most important discovery for understanding the deep geodynamics of the Earth was the system of ascending mantle plumes discovered from seismic tomography data in the late 1970s. This method ultimately yields three-dimensional distribution models for propagation of seismic velocities for compressional (*P*) and shear (*S*) waves in the body of the Earth from natural sources—earthquakes. One of the first experiments on using travel times from strong seismic events to reconstruct lateral velocity inhomogeneities in the mantle is [1] within the Pamir–Baikal profile. Development of the global seismological network and access to a huge amount of data gave rise to seismic tomography as a new type of global studies of the Earth's mantle, for which [30] is considered pioneering. In seismic tomography, lateral velocity variations in the mantle

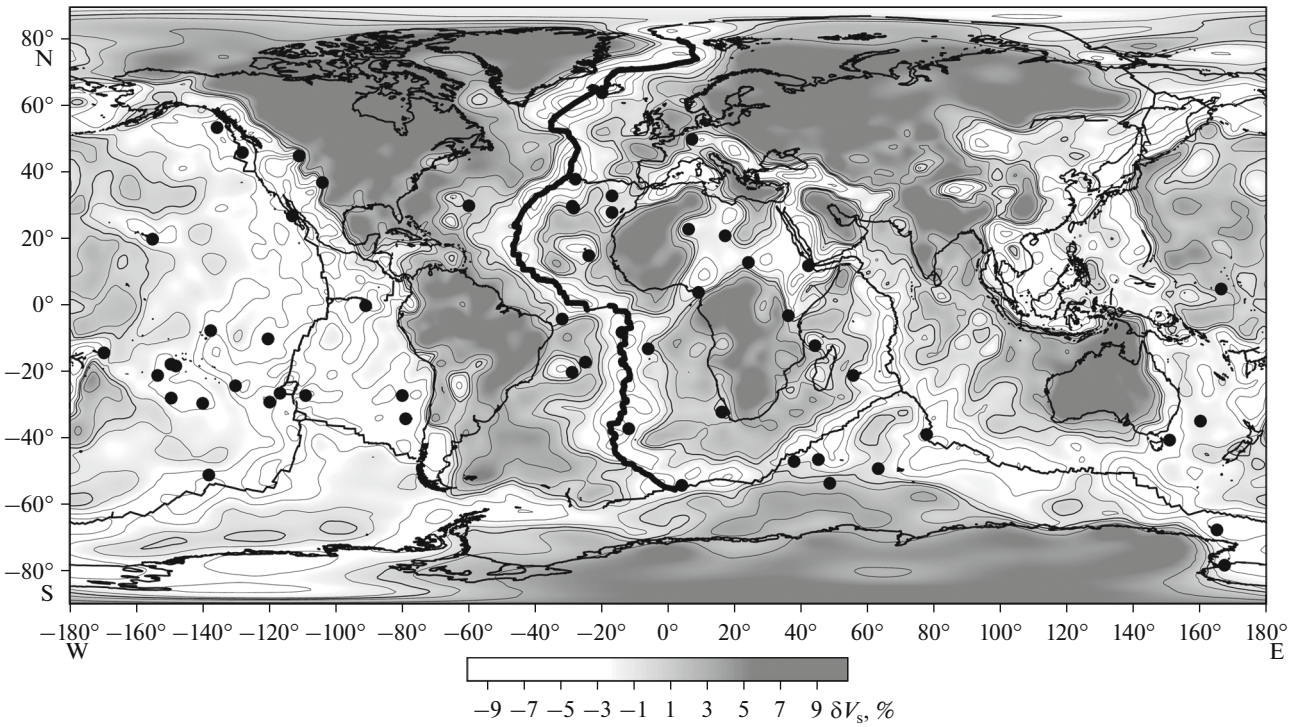

Fig. 1. Horizontal slice of seismic velocity variations δV_S of SL2013sv volumetric tomographic model, after [47], at a depth of 100 km. Isoline step, 2%. Shown: axis of MAR along which sections are plotted (bold line); system of mid-ocean ridges and outlines of continents (thin lines); position of hot spots (black dots), after [26].

δV with respect to the average values are selected in order to minimize the residuals of travel times, which are calculated as the difference between the measured and theoretical wave arrival times based on a first-approximation radially symmetric velocity model.

Seismic tomographic models reflect the geodynamic state of the mantle space and its rheology [33]. Negative variations in δV are interpreted, as a rule, as a consequence of the heated and partially molten state of the Earth's interior, where local velocities decrease. Positive variations in δV are interpreted as cold material of ancient cratons or slabs subducting from arc zones. This interpretation of δV, conditionally called "thermal," is generally accepted. In a comparative review of various mantle models [23], this approach is demonstrated as the basic one for most researchers. Note that in addition to the thermal, there is also a material dependent mechanism for the formation of variations in δV and "strain sensitivity of the medium" [14], but at present their use for interpreting mantle inhomogeneities beneath the ocean is not the main one.

The main discoveries of global seismic tomography are as follows. From *S*-waves, a system of negative anomalies has been revealed for the Earth's surface layer, associated with mid-ocean ridges and hot spots, which are local intraplate outlets of plume branches to the surface (Fig. 1). Cratons are represented by a homogenious positive field δV_S, except for hotspot zones (e.g., East Africa). A review of the volumetric distribution of velocity variations shows that the obtained pattern differs from the expected scheme with ascending flows along the boundaries of convective cells under mid-ocean ridges (Fig. 2). At depths exceeding 300 km, the mid-ocean ridge system in the field δV_S decays and it is impossible to trace the presence of a single anomaly associated with an ascending convective flow in a divergent zone of the Earth. According to D. Anderson [21], this was confidently revealed based on seismic tomography data in the late 1980s. Mid-ocean ridges are considered as structures that occurred from a passive response to plate divergence, but not as a marker of ascending deep mantle flows along the boundaries of convective cells [21]. Intense isolated anomalies are observed on the horizontal section, which are the roots of the African and Pacific superplumes; the roots of superplumes start from the mantle–core boundary and rise to the surface as smaller discrete branches (Fig. 2). These branches on the surface form hot spots and, in some cases, overprint mid-ocean ridges, having deep roots, e.g., in Iceland (Fig. 1). Researchers have repeatedly emphasized that the near-surface branches of superplumes in plan view are tied to the outer contour of the periphery of their roots [26] (Fig. 2).

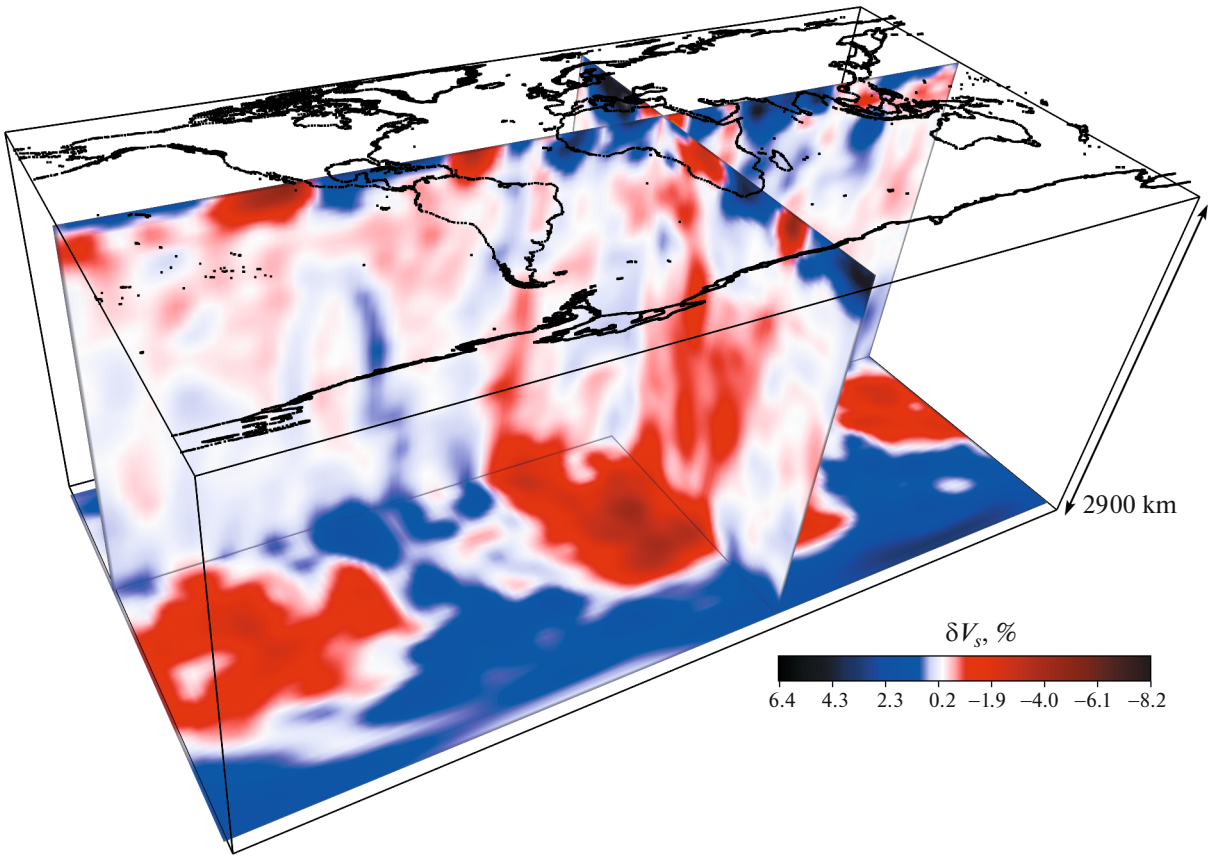

Fig. 2. Volumetric distribution of seismic velocities δV_S 31st-order NGRAND tomographic model (after [23, 27]) on block diagram along three mutually perpendicular sections above mantle–core interface (2770 km), meridional (32° E) and latitudinal (30° N). Vertical scale is exaggerated 1: 6 than horizontal.

The main thing demonstrating the primary analysis of thermal hot anomalies is the absence of continuous anomalies locked in a cell under divergent boundaries, ascending from the core–mantle boundary to the surface. Continuous negative anomalies under mid-ocean ridges in data of the late 1990s are not traced deeper than 300 km [23, 27, 47] (Figs. 1, 2). It is possible for branches of the Pacific superplume to flow under the Mid-Atlantic Ridge (MAR) (Fig. 2). According to new data from Lebedev et al. [40], an axial negative velocity anomaly is not traced deeper than 200 km, which brings the position of its base closer to the solidus depths under the MAR axis, where the processes that form seismic velocity anomalies begin. Anomalies associated with superplumes are in the form of ascending and branching columns that do not coincide in spatial position with classical divergent plate boundaries. This type of heat transfer from the bottom to the upper mantle, of course, is part of a heat engine, which does not function at all as assumed before the advent of the seismic tomography method. One way to adapt the convection model to reality is by introducing stationary two-layer thermal convection [11]. In this case, the structure of superplumes from the core to depths of ~700 km is explained, and a separate layer with convection phenomena is assumed for the upper part of the mantle, which receives pumping from the lower layer. In the upper layer, to ensure the movement of plates, the mechanism of convective rolls should operate [7], but practically in the oceanic part of the section, with the existing resolution of the method, no signs of it are observed.

Thus, the MAR zone is in no way represented as a deep anomaly of heated material comparable in scale to the depth of mantle and a plate-drift generator (Fig. 2). Branches of superplumes are comparable anomalies, but they melt pointwise through the lithosphere, creating zones of weakness and chains of volcanic edifices, and are not defined as a source of plate movement. For the Cape Verde Islands hotspot, the African Plate is “anchored” to a large branch of the African superplume, and magmatism in this system has formed spatially nonmigrating volcanic edifices since the Upper Cretaceous [12] (Fig. 2). In the case of particularly large sizes of the upper parts of superplumes, local currents form that can laterally transport lithospheric blocks, but not plates [19]. for the Atlantic is irrelevant due to the absence of extended subduction zones with inclination from the MAR, the slab pull

into which could have been the mechanism for the opening of this ocean. The asthenospheric current, as well as manifestations of currents in other shells, should create the well-recognized dynamic relief associated with MAR. However, based on the data of [37], the dynamic relief, which is part of the residual relief, in which the isostatic influence of lithospheric masses has been removed, is associated not so much with the MAR as with areas where plume branches reach the surface (Iceland, the Azores, the vicinity of Bouvet Island).

Since the beginning of the 1980s, the seismic tomography method has been intensively developed by improving the network of seismic stations and mathematical apparatus for data processing. This has continuously improved the resolution of the method for identifying mantle velocity inhomogeneities. In parallel, compared to surface data, an interpretation of their genesis was developed and a comprehensive pattern of tectonic processes and structure formation in the tectonosphere of the entire Earth was formulated. The MAR is of particular interest as a divergent boundary between the flanking plates passing into the Arctic. This is the most studied segment of the global system of ridges, in which many tectonic phenomena characteristic of areas of new oceanic crust formation are manifested, including the superposition of superplume branches on the MAR, the existence of which was revealed by seismic tomography data. This method also showed that under the MAR, the axial negative velocity anomaly has a variable depth, which correlates with a number of geological and geophysical characteristics.

This study considers the features of tectogenesis along the MAR in the presence of a shallow mantle heterogeneity, identified by the position of the along-axial hot tomographic anomaly, by comparing and correlating it with surface geological and geophysical parameters of various nature. We also consider the evolutionary aspect of ideas about the MAR zone and relationship between the deep structure and surface data. We present a modern view on the correlation of these data with mantle heterogeneities available for study using seismic tomographic models of the mantle.

DEVELOPMENT OF THE LEVEL OF DETAIL OF SEISMOTOMOGRAPHIC MODELS

The detail of global models of mantle velocity variations depends on the number of spherical harmonics used for spectral representation of the velocity variation field. The first models in the 1970s and 1980s contained up to 12th- and 16th-order harmonics. At the turn of the 2000s, 31st-order models were used for global variation pattern. Modern regional models use higher-order harmonics [8] or parametrization values three to six times more detailed. Obtaining regional models is effective in highly seismic areas with a dense seismological network, e.g., along Pacific subduction zones. Global models are mainly used to analyze mantle heterogeneities along the MAR.

The first seismic tomography studies of the mantle containing 3D velocity variation models with a level of detail up to 12th-order harmonics, which appeared in the late 1980s [31, 50], showed an axial negative anomaly of mid-ocean ridges to depths of 400–670 km. Models with up to eighth-order harmonics [44] revealed a significant uncertainty in velocity variations in the middle mantle from 900 to 1800 km, and it was proposed that they be interpreted as a consequence of large-scale convection processes spanning the entire mantle. However, 3D visualization of these models showed that negative anomalies under the system of mid-ocean ridges at this resolution begin to isolate and probably do not have deeper roots. Modern 3D models with up to 12th-order detail, which are already used as a first approximation for calculating velocity variations instead of the radially symmetric PREM model, show what the mantle space looks like in this limitation in the level of detail [32, 38, 45] (Fig. 3). The negative anomaly under the MAR has a depth of at least 400 km. It is also traced more deeply in the form of a lens between discontinuities at 400 and 670 km. The section across the North Atlantic according to SP12RTS-S model data can be interpreted in two ways (Fig. 3). On the one hand, deeper than the 670 km boundary, a hot negative anomaly was revealed up to the mantle–core boundary, which may be associated with the ascent of material along the contour of a convective cell. On the other hand, it is now known that this anomaly is a spatially limited branch of the African plume, but due to the low resolution of the model, it is extremely difficult to differentiate these anomalies (Fig. 2).

In the early 1990s, the absence of deep roots of negative anomalies of mid-ocean ridges gave rise to new approaches for deep mantle geodynamics [21]. Nevertheless, since the main results were expressed by models with low detail, in which the real sizes of mantle inhomogeneities were overestimated, the viewpoint of their structure as a reflection of the general mantle convection still prevailed [48]. Analysis of individual features of velocity anomalies in the areas of the Iceland and Afar branches of the African superplume using models of various levels of detail showed clear spatial separation of plume branches, shallow axial anomalies of the MAR, and slabs as the main objects of the mantle's thermal structure [45, 49]. As well, there is no system of convective cells among them. The relationship of surface geodynamic processes manifested in geological and geophysical characteristics with the deep rheological state of the mantle and the dynamic surface relief associated with it, corrected for isostatic effects, has been proven [33].

The correlation of geological and geophysical parameters along the MAR with tomographic data reflecting the rheological state of the upper mantle is very effective as an approach for geodynamic interdis-

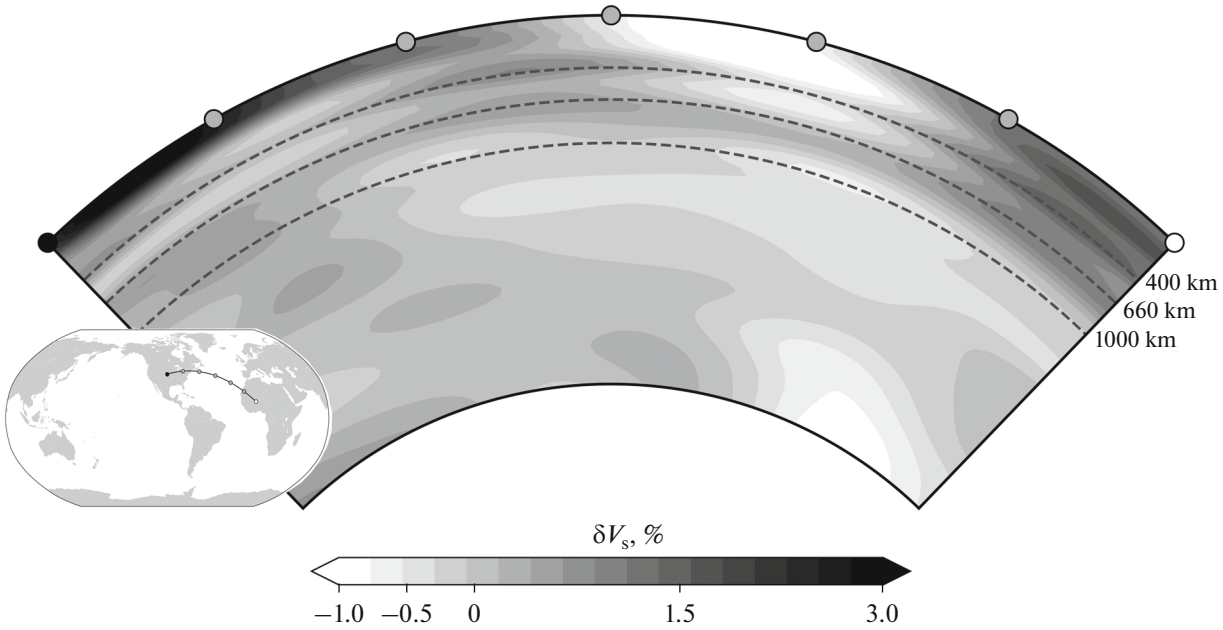

Fig. 3. Seismic tomographic section o mantle orthogonal to MAR in North Atlantic calculated from data of SP12RTS-S model (after [38, 45]), which contains 12th-order spherical harmonics. The section was constructed with the SubMachine program [36].

ciplinary study of the structure. One of the first to use this approach was E. Bonatti [3], who, when comparing the structural features of the axial part of the Atlantic with seismic tomography data, revealed that large fault zones with a length of the active part of >200 km are spatially adjacent to cold upper mantle blocks. Two versions of this have been put forward:

— cooling of the mantle through a macrofractured medium;

— the initial presence of long-lived cold blocks, along the boundaries of which large fault zones appear.

As a result of analysis of the aggregate data, a conclusion was made in favor of the second version. To obtain this result, we used a seismic tomographic section along the MAR according to the RG5.5 model with parameterization on 5° × 5° cells [54]. This made it possible to determine cold zones in the equatorial segment and at latitudes of approximately ±50°. The RG5.5 model was a great achievement in terms of detail: up to 36th-order harmonics were processed, but not to the entire depth of the mantle, only down to 500 km (Fig. 4). The detail in the MAR zone for variations in *S*-wave velocities was supplemented by data on the phase and group velocities of surface waves, which yielded a qualitative leap for models of this type in areas with low seismicity and low density of the seismological network. The section along the MAR shows that the axial anomaly does not descend deeper than 300 km, and in places where the branches of the African superplume (Iceland, the Azores, and Tristan da Cunha) overlap it, the depth of the base of the axial anomaly is greater than the average for the section (Fig. 4, anomaly *3*). The resulting model led to the most important conclusion that under the MAR axis and in plumes, two different types of upwelling occur: active plume and passive axial, arising as a response to stretching and a decrease in lithostatic pressure during the divergence of lithospheric plates [54]. However, the sources of plate movement are debated by researchers today and, judging from the discussion in the modern literature [25], the matter is still open.

The section clearly shows three minima corresponding to superposed plume branches (Fig. 4, anomaly *3*). Variations in seismic velocity govern density variations in the mantle and, accordingly, in the gravity field on the surface. Comparison of the section with the data of free air and Bouguer gravity anomalies shows that the low-frequency components of these fields coincide in the location of extended anomalous zones with the minima of the seismic tomographic section, represented by decompacted mantle zones (Fig. 4, anomalies *1*, *2*). Zones with heated and decompressed matter in Bouguer anomalies, which are the deeper, the deeper the roots of mantle anomalous zones. Since the productivity of magmatism is particularly high in these zones, the relief formed by basalt flows has an increased value and is depicted by maxima in the free air gravity field. Thus, the geophysical characteristics obtained along the MAR at the level of extended (>500 km) anomalous zones in the section have an antiphase behavior and a consistent physically substantiated interpretation owing to the rheological state of the mantle revealed by seismic tomography (Fig. 4, anomalies *1*, *2*). The configuration of negative

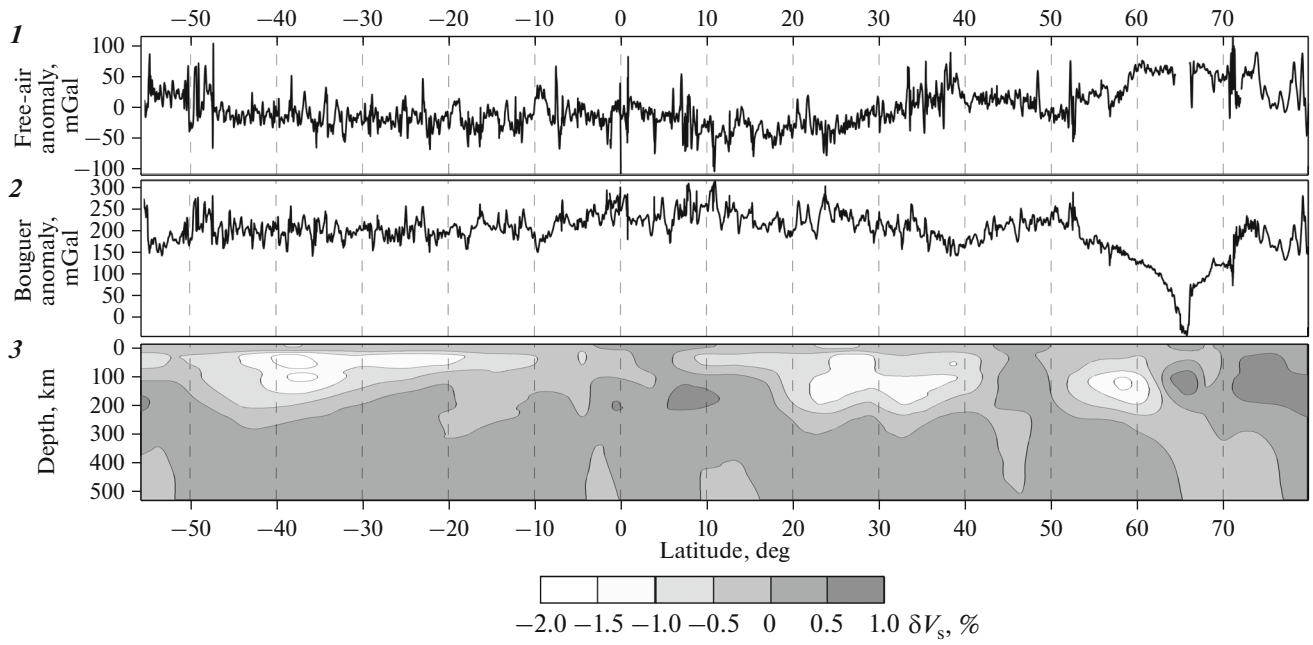

Fig. 4. Correlation of geophysical fields along MAR axis (after [42], with changes and additions). Position of section along MAR is shown in Fig. 1. *1*, free air gravity anomaly based on satellite altimetry, after [46]; *2*, Bouguer anomalies; *3*, section of variations in shear wave velocities according to data of seismic tomographic model RG5.5 (after [54]) in upper mantle (0–500 km).

tomographic anomalies in the northern segment of the MAR is formed of branches from a deep conduit directed to the south, indicating along-axial flow of heated masses. This is confirmed by data on the southern migration of the Azores plume [24, 29].

At the end of the 1990s, the NGRAND model of mantle velocity variations appeared with a level of detail up to 31st-order harmonics, calculated for its entire depth [23, 27]. In our study, we present a section constructed from this model (Fig. 5). The depth of the MAR axial anomaly, like in the RG5.5 model, is no greater than 300 km. As well, throughout the entire mantle space up its boundary with the core, one can clearly see the separation of anomalous hot zones based on types of upwelling into passive-axial, which has no deep roots, and active-plume: this separation of anomalous hot zones based on types of upwelling is the most important result that led to the concept of deep geodynamics [54]. The location of the section was chosen in the southern segment of the MAR, which is a classical one for illustrating plate tectonics theory; the section shows a branch of the African superplume ascending to the surface with displacement to the east (Fig. 5). From a cold barrier from 700 to 400 km, it reaches the surface and is manifested in formation of the Réunion hot spot with an anomaly of almost −5%. An interesting feature of the section is the presence of isolated hot anomalies in the depth range from 1000 to 1600 km, which are symmetrical with respect to the MAR to local anomalies within the superplume branch in the same depth interval (Fig. 5). For a possible interpretation of this picture, one could theoretically use the mechanism of capture by the lithosphere in the MAR zone of the top of the superplume branch and its pulling away from the MAR during plate drift, by analogy with the segment in the area of the Cape Verde Islands and the Kane Fault [12]. But in this case, the symmetrical anomalies are located deep and one would have to consider too large volumes of the mantle involved in the horizontal movement. A more realistic explanation is that these anomalies to the west of the MAR appeared when the plane of the section crossed some eastern branch of the Pacific plume. Symmetrical location of the minima within the branches indicates that the intensity of the ascent of heated matter up the plume branch is impulsive, which is almost synchronous for other branches of superplumes for the entire Earth [17, 20].

The new class of models that appeared in the 2000s has a resolution higher than its predecessors. The MITP08 model has a variable resolution and the size of the spatial resolution in areas with strong seismicity and denser seismological networks reaches 50 km in both the vertical and horizontal directions [41]. This model is calculated from *P*-waves and in oceanic areas, where the seismicity is an order of magnitude lower than in subduction zones and continental collisional belts; its resolution differs little from the 1990s models.

The SL2013sv model was calculated from *S*-waves for the upper 700 km of the mantle using surface waves in a wide range of periods to obtain additional information on *S*-wave velocities in regions with relatively low seismicity, in particular, the MAR region [47].

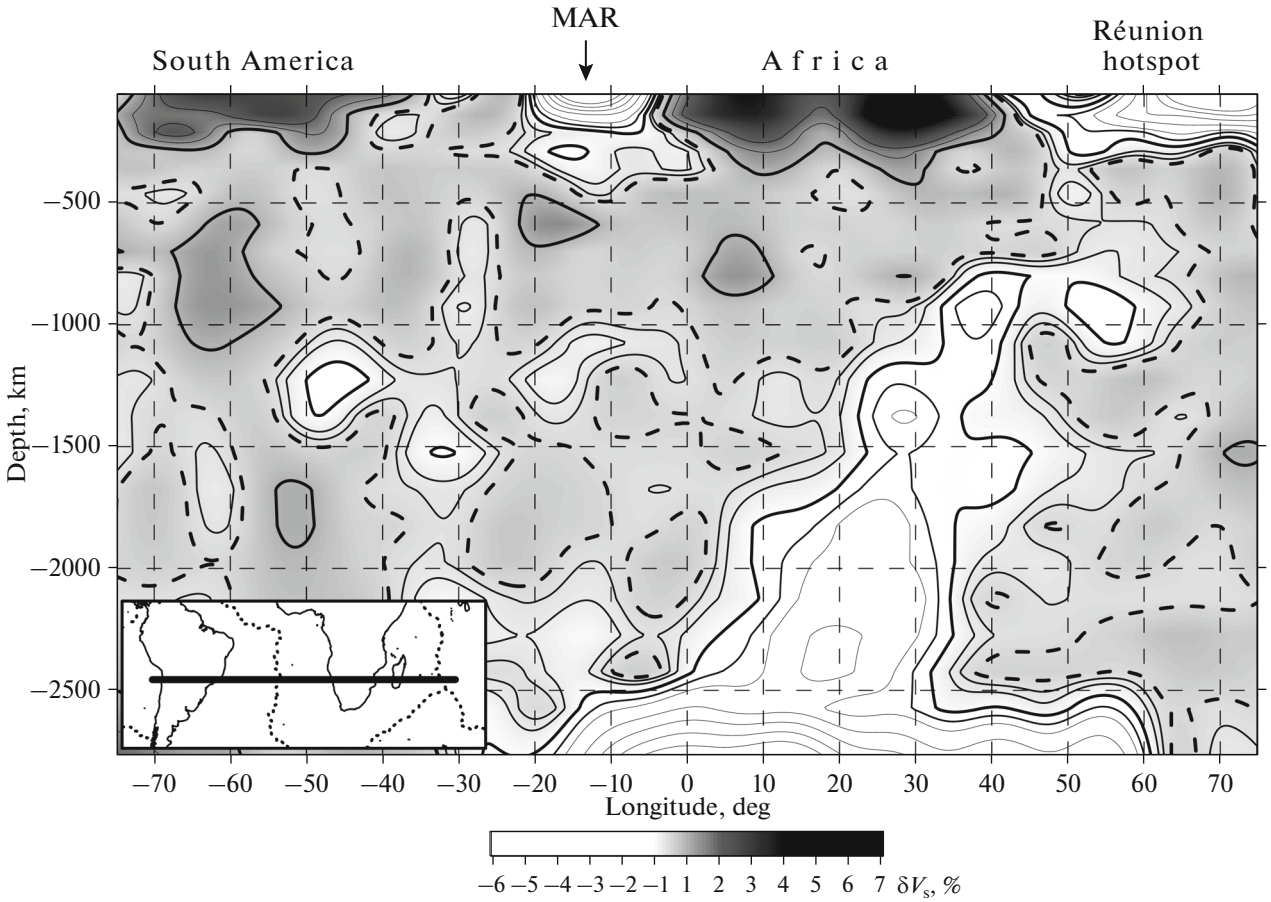

Fig. 5. Section of δV_S seismic tomographic NGRAND model across South Atlantic from surface to mantle–core boundary (after [23, 27]). Shown: position of section (inset); zero isoline (dotted line); isolines are drawn with step of 0.5%; isolines ±0.5% clipping background values for used data are given with increased thickness.

This model shows the depth of the hot zone under the MAR to be ~120 km, which is even closer to the solidus depth [47]. Deeper, the axial anomaly is not observed (Fig. 6, section *2*). However, reliable δV_s, values determined from a value of less than −1% are located at depths of ~200 km. At depths of 100–120 km are the most heated areas of the axial anomaly with a value of less than −5%, which probably indicates the most productive magmatic segments of the MAR. A model of this type can possibly be used for a comparative analysis of new seismic tomography data with geochemical parameters reflecting the deep characteristics of mantle material, melt separation conditions, and the geochemical nature of mantle sources.

For certain basalt glasses, L.V. Dmitriev et al. [6] calculated in the PETROLOG program the pressures and corresponding depths of magmatic melt separation from mantle sources of MAR magmatism [28]. Comparison of the these values for the plume association of basalts with the section shows that the configuration of the lower boundary of the point cluster has three areas with distinct sinking: the Icelandic, Azores, and South Atlantic plume anomalies (Fig. 6, profile *1*). They significantly correlate with the shape of the foot of the negative anomaly along the MAR, which for *S*-waves indicates a heated and partially melted state of the mantle. Comparison of these data shows that tomographic models of the upper mantle with the modern level of detail can already be used for comparison with geochemical characteristics and prediction in areas without sampling oceanic basement rocks. The SL2013sv global model is currently the most objective for comparing the rheological state of the mantle with basalt and peridotite isotope data [51]. According to the SL2013sv model, cold mantle blocks are close to the surface in the same zones as in the early NGRAND model, but at depths of 250–300 km (Fig. 5). It also indicates that the depth referencing of the resulting conclusions when working with more detailed models can be adjusted upwards depending on the new resolution values. This is because mantle irregularities of fixed size, depicted by a longer wavelength field, look larger than their true sizes. This has gradually been corrected with the increasing resolution of the data, as shown by comparison of the depicted

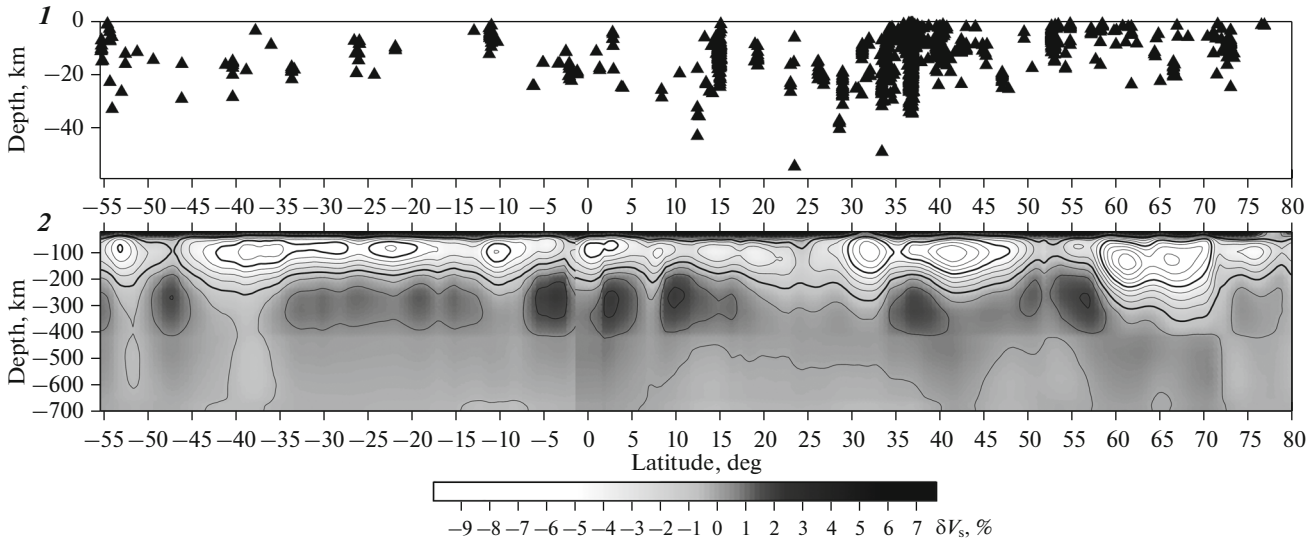

Fig. 6. Distribution of geochemical characteristics of basalts and seismic velocities along MAR axis from −55° to 80° N. Position of section along MAR is shown in Fig. 1. *1*, depths of separation of basalt melts of plume association TOP-1 along MAR axis, after [6]; *2*, section of velocity variations δV_s of SL2013sv model along MAR axis, after [47].

depth of the MAR axial anomaly on models with different levels of detail.

Despite the complexity involved in calculating a regional model along the MAR based on shallow (no deeper than 30 km) and weak (magnitude no more than 4.0) seismic events, an algorithm was created that can calculate such models [39]. The first results with this algorithm as applied to the MAR showed that it can be used to construct a section of *P*-wave velocity variations on a regular grid over a few tens of kilometers to depths of 400 km in a ±500 km strip from the middle ridge [9]. For the Central Segment of the MAR, the data also showed that the axial anomaly, previously seen as a continuous zone of negative δV anomalies in the horizontal direction desintegrates into a series of subvertical lenses from the surface to depths of 200 km with a width no greater than 50 km [9] (Fig. 6, profile *1*). The increased level of detail shows how the heated and partially melted mantle regions under the MAR actually look in the velocity field, which previously, when studied by low-resolution methods, merged into a single deep (up to 700 km) negative δV anomaly, which according to the theory is due to general mantle convection. Desintegration of a single axial anomaly into a chain of vertical lenses under slow spreading conditions corresponds to geochemical data on the discrete manifestation along the MAR of basalts of different petrological associations with different melt separation depths, which get mixed during faster spreading [5]. Confirmation of this phenomenon using the tomographic data of regional models along the MAR, constructed by the algorithm, is currently the most advanced implementation of this method for the boundaries of divergent plates based on weak teleseismic events [39]. A more detailed structure of velocity variations in the MAR region can only be obtained from the data of locally deployed ocean bottom seismographs.

DATA ANALYSIS ALONG THE MID-ATLANTIC RIDGE (MAR)

Data Comparison

Based on a description of the evolution of the tomographic data and their correspondence to phenomena observed on the surface, we assume that deep mantle heterogeneities due to the difference in thermal state are the main source of geodynamic processes. They determine the configuration of the main tectonic elements and spreading rates. To correlate these characteristics, we compare them with the section of variation in the velocity ratio $\delta(V_p/V_s)$, calculated with the NGRAND and HWE97p models [16, 23, 7, 53] (Fig. 7). These models were chosen for calculating the attribute $\delta(V_p/V_s)$ because for different types of velocities they had the maximum possible, as well as a comparable level of detail [16]. These conditions are necessary for calculations with the division of one parameter by another in order to avoid artifacts. Cold anomalies in the upper mantle along the MAR were revealed at an average depth of ~500 km for models with 31st-order harmonics, coinciding in the Equatorial and North Atlantic with areas of maximum sublatitudinal displacement of the MAR zone (Fig. 1; Fig. 7, profile *5*, dotted line). For the attribute $\delta(V_p/V_s)$, these anomalies have the physical sense of a zone with minimum Poisson ratios, at which the rheological state of the medium differs to the maximum from the mobile and effectively fluid state in the hot

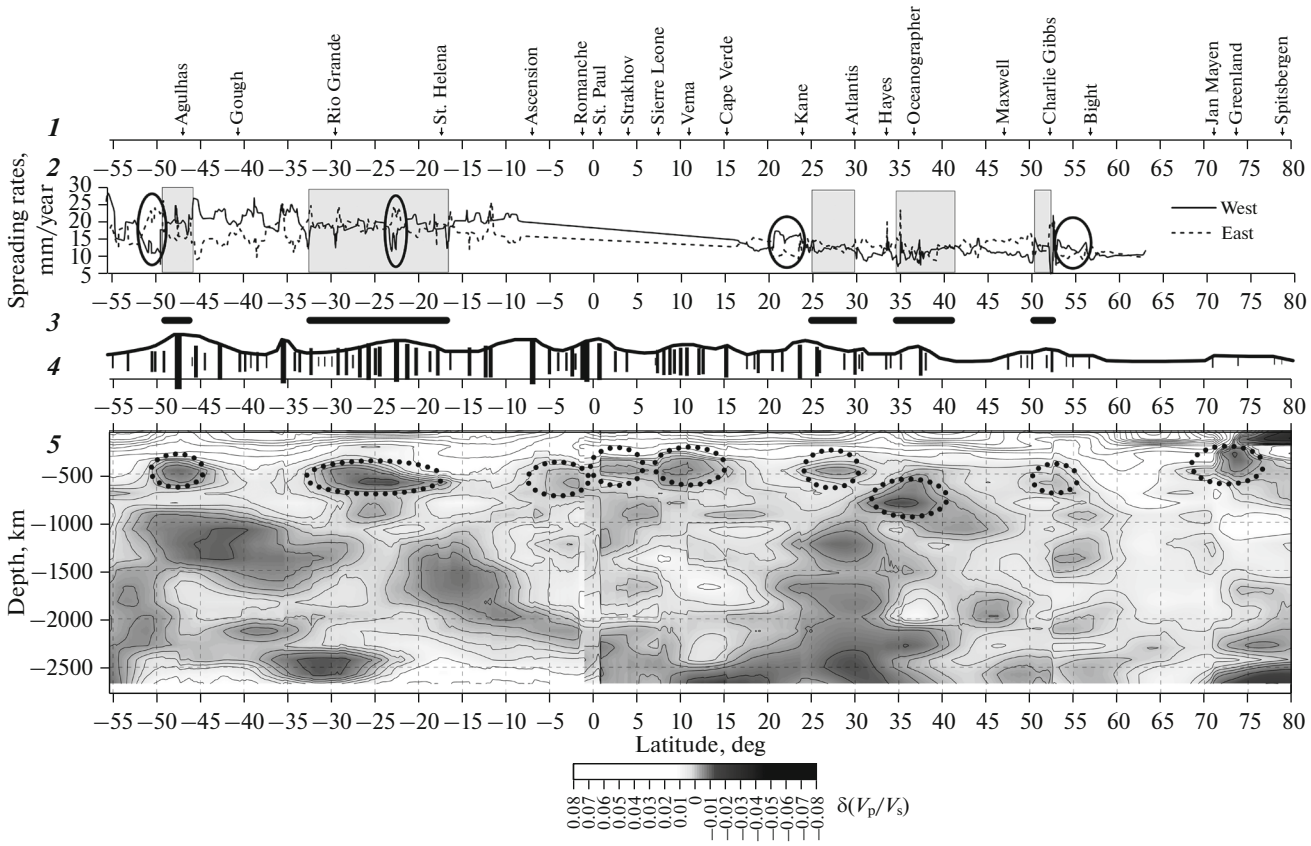

Fig. 7. Correlation of geological and geophysical parameters along MAR axis, (after [16], with changes and additions). Isolines of attribute are given through 0.01. Inverse regions with strong predominance of eastern half-rates in Southern Hemisphere and western half-rates in Northern Hemisphere (ellipses); western flank of MAR (solid line); eastern flank of MAR (dashed line); cold upper mantle anomalies of Atlantic under MAR axis (dotted circles). *1*, position on MAR axis of intersections with largest faults and their names; *2*, spreading half-rates (mm/yr) along 4 Ma isochron for western and eastern flanks of MAR, constructed after [43] with interval from 8° S up to 15° N due to low reliability of values obtained in it; *3*, position of zones with minimal west–east asymmetry of spreading half-rates for areas with reliable identification of linear magnetic anomalies; *4*, position of intersections of transform faults with MAR with size of symbol linearly proportional to total length with passive parts, and their envelope (after [15]); *5*, variations in attribute $\delta(V_p/V_s)$, calculated from seismic tomographic data for *P*- and *S*-waves, after [23, 27, 53].

axial anomaly of the MAR to depths of 300 km, or in plume zones. The total lengths of sublatitudinal transform faults are given along with their enveloping curve [15] (Fig. 7, profile *4*). In addition to the uneven density of these structures along the MAR axis, analysis of their quantitative characteristics is related to deep mantle heterogeneities.

The spreading rate is most important parameter during geodynamic processes governed by mantle heterogeneities. The spreading half-rates along the 4 Ma isochron are shown as a pair for the western and eastern flanks of the MAR, plotted according to [43] without the interval from 8° S to 8° S up to 15° N (Fig. 7, profile *2*). Since the equatorial segment contains a highly fragmented anomalous magnetic field, no reliable linear anomalies have been identified in this interval, and the half-velocity calculation errors are too large. The data show a smooth increase in the spreading rate with increasing distance from the pole of rotation of the plates separated by the MAR (about 60° N). On this background, local half-rates variations occur, reaching 100% along the strike of the MAR and up to 250% in the difference between the western and eastern flanks. The sizes of segments with local variations in half-rates are comparable with the depths of the roof of cold lenses, which confirms the possible comparability of the depths of mantle structures with surface structures in terms of scale and substantiates the choice of these parameters for analysis (Fig. 7, profile *5*).

In this study, we used a database of teleseismic events [22, 52]. Moments of seismic events were summed over 1 segments of the MAR using the empirical formula for the Atlantic [2]. All types of magnitudes were used for the calculation, since the most reliable determinations of M_w make up about 10% of all events, but the estimate in this case is greatly understated. The total moment in accordance with the determined and assigned focal depths were calculated for three depth intervals: 0–13, 13–35, and >35 km (Fig. 8).

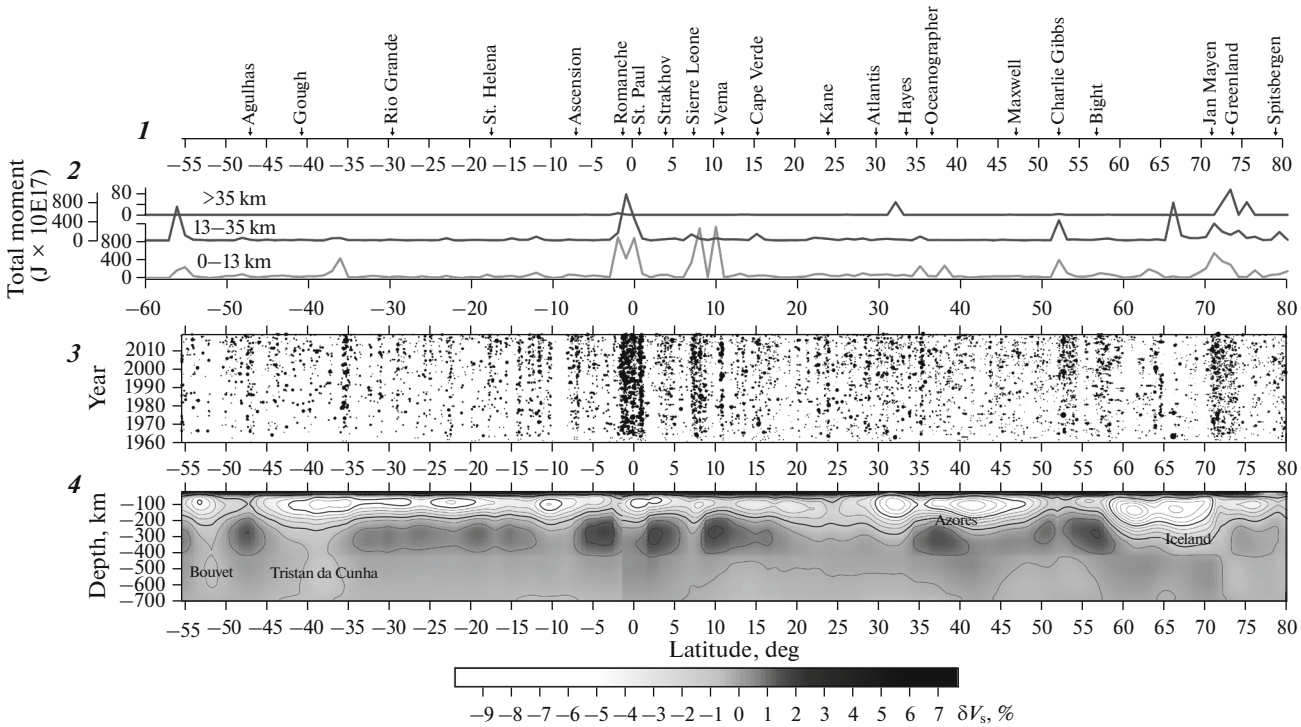

Fig. 8. Correlation of seismicity along MAR axis with seismic tomographic data. *1*, position on MAR axis of intersections with largest faults; *2*, total seismic moment along axial zone of MAR, calculated from data [22, 52] for all types of magnitudes after method [2] for three depth ranges: 0–13, 13–35, and >35 km (after [4], with additions); *3*, spatiotemporal depiction of seismic events along MAR axis, starting from 1960—sizes of symbols are proportional to magnitude and events positions are given in projection onto latitude axis (after [22, 52]); *4*, section of velocity variations δV_s of SL2013sv model along MAR axis, after [47]. Position of section along MAR is shown in Fig. 1. Names of branches of African plume are given.

DISCUSSION

Interpretation of the Compared Results

Comparison of the seismic tomographic section along the MAR and correlation of surface geological–geophysical characteristics of various natures forms a consistent system of interconnected geophysical fields and their deep sources and bottom structures. In the Equatorial and North Atlantic, compact fault groups are located above cold upper mantle anomalies in places of maximum sublatitudinal displacement of the MAR (Figs. 1, 7, profiles *4*, *5*). The most striking example of such displacement is the pair consisting of the Romanche fault and São Paulo polyfault system. North of 7° N, this displacement above the cold block of upper mantle is represented by a sequence of fault systems, including the Vema fracture zone. In the North Atlantic above a cold anomaly, the MAR is displaced along the dual Charlie–Gibbs fracture zone. Thus, a large displacement above the cold mantle can be expressed by ordinary transform displacements, but more often it breaks up into twin and polyfault systems.

The density of MAR transform faults and their lengths, emphasized by a pseudoperiodic "pulsating" shape of the envelope with an average step of about 12° (1320 km), along the MAR correlates with the positions of cold lenses (Fig. 7, profiles *4*, *5*). This step is comparable to the depth of cold lenses in the upper mantle from 500 to 1500 km. It is also possible that the parameters correlate on a shorter period scale, but at the moment, there are no detailed data for this along the entire length of the MAR. There is also a longer-period correlation of geological and geophysical parameters along the MAR in manifestation zones of the Azores and Icelandic plumes, in particular, between the Bouguer anomalies and hot anomalies in the upper mantle (Fig. 4). Modulations of the total lengths of faults and their referencing to cold lenses demonstrates their direct influence on macrofracturing of the lithosphere in the vicinity of the MAR. This effect is manifested not over cold lithospheric blocks, but over cold sublithospheric lenses. The geodynamic influence on the degree of tectonic fragmentation of the lithosphere is formed by the thermal state of the mantle in a layer about 300 km thick directly above the 670 km section. Fragmentation persists when the transform zones with distance from the MAR during spreading. For the MAR zone, this is because the sublithospheric layer may be involved in lithospheric plate movement, increased friction of the bases of which near cold lenses creates a condition for increased macrofracturing. In the space between lenses, the mantle is less viscous and the number of large faults, as well as their

length, decrease. When more detailed tomographic data are obtained, the depths of the cold lenses can be corrected upwards.

Studies of the spreading rates along the MAR and its flanks along different isochrons showed that they contain more than twice as many discrepancies in the kinematics of neighboring spreading segments separated by transform faults [13]. In this situation, within the plates orthogonally to the MAR, horizontally differentiated displacements and shear deformations will occur not only in the active parts of faults, but also the passive areas far from the rift zone due to an additional shear component arising from the difference in velocities. This will be reflected in the nature of seismicity. In the velocity distribution, traditionally estimated from values in one direction from the MAR and defined as half-rates, there is also an asymmetry on the western and eastern flanks (Fig. 7, profile *2*). The asymmetry decreases almost to zero on some segments of the MAR, the position of which is referenced to cold lenses and modulation maxima of transform faults envelope (Fig. 7, profiles *3*, *4*). This observation confidently demonstrates that in these segments of the MAR, the lithosphere and sublithospheric space are interacting with cold lenses, forming the symmetry of the half-rates and increasing the fragmentation of the lithosphere. These geodynamic consequences can be explained by the interaction of mantle regions with different rheological properties in the vertical direction. However, there may be another interpretation. Between cold lenses, the spreading half-velocity asymmetry reaches its maximum values. Therefore, the mantle geodynamics over cold lenses may be a standard background phenomenon, and hot zones, which are offshoots of superplumes, are exceptions to the rules in which, due to the reduced mantle viscosity, a degree of freedom of movement of plate fragments occurs, with the rates of one of the MAR flanks prevailing. (Figs. 2, 5). Within the plate are segments with different kinematics and predominant direction of the spreading process (horizontal keypad). The segments of the MAR have different kinematic characteristics independent of each other, which indicates a nonuniform and nonrigid structure of the plates and possible independent movement of parts within them. These processes are intensified in areas between the cold lenses and in places where deep branches of plumes enter the MAR.

The half-rates of the western flank of the MAR in the Southern Hemisphere are greater than of the eastern flank, and vice versa, in the Northern Hemisphere, the half-rates of the eastern flank predominate over the western (Fig. 7, profile *2*). Taking into account the existence of a common western plate drift component [18], the fixed position of the African Plate with respect to the deep sources of magmatism in the Atlantic [12], and the general sublatitudinal displacement of the North American Plate to the west according to [34], the prevalence of eastern half-rates of the MAR in the Northern Hemisphere can be explained by the following process. As it moves, the North American Plate, which has a rigid connection between the continental and oceanic parts, also moves the active rift frame of the MAR from the fixed African Plate, which creates conditions for faster spreading crustal thickening on the eastern flank of the MAR. In the Southern Hemisphere, the pattern is the opposite. Since the current latitudinal velocity component for the South American Plate according to [34] is almost zero, and the southern part of Africa has a small eastern component of the total motion vector, the half-rates on the western flank of the MAR predominate. The opposite effect of the overall asymmetry of spreading half-rates along the MAR in the Northern and Southern hemispheres indicates the effects of the Earth's rotation on the geodynamics of the described processes, and, possibly, the Coriolis effect, but the study of this influence is beyond the scope of this work.

A comparison of the half-rates profiles for the 4 Myr isochron shows that there are segments where the predominantly western (or eastern) predominant half-rates undergo a local inversion in the corresponding hemisphere (Fig. 7, profile *2*). These inversions are spatially located in both hemispheres at approximately the same latitudes: between 20° and 25° and around 50° and 55°. These values are located towards the poles and the equator from the critical latitude 35°16′, which is important for the geometry of tectonic processes on a rotating spheroid [10]. This observation demonstrates the need to take into account rotational mechanisms in constructing geodynamic models of the Earth. In addition to the actual rheological state of the mantle, rotational effects constitute the additional factor of tectogenesis, the superposed action of which forms the modern appearance of structures and processes.

The main manifestations of the total seismic moment along the MAR were noted in zones with maximum lateral displacement of the rift structure axis (Fig. 1; Fig. 8, profile *2*):

— demarcation faults of the Equatorial Atlantic—the Romanche and São Paulo group from the south and 15°20′ from the north with a total displacement amplitude of about 3300 km;

— the Mohns and Knipovich ridges between the Arctic and North Atlantic with a total displacement amplitude from the MAR of about 950 km;

— The Charlie–Gibbs polyfault system with a displacement amplitude of about 350 km.

The rest of the MAR space is represented by weak background values associated with spreading magmatism and has a moment an order of magnitude lower than the shear zone maxima. The distribution shown in some cases is violated by an increased total moment of events in plume regions: Bouvet, Tristan da Cunha, Azores. and Iceland. The distribution of the total moment shows that the maximum geodynamic activity

of the MAR rift structure, which consists of a combined spreading segments and transform faults, is concentrated in shear tectonic elements (Fig. 8, profile *2*). The maximum energy release occurs in geodynamic conditions unassociated with the generation of new crust when plates diverge from an extended divergent boundary. Demarcation fault zones are located above cold mantle lenses in the presence of a contrasting lateral transition to hot mantle areas (Fig. 8, profile *4*). This shows that the maximum crustal fracturing and accompanying seismicity arise during interaction of mantle segments having different rheological states.

The distribution of the total moment along the MAR was calculated for three depth intervals (Fig. 8, profile *2*). The >35 km interval contains few events. In the 0–13 and 13–35 km intervals, an almost synchronous moment distribution is observed, but there are a number of minor discrepancies. In the region of plume branches in the 0–13 km surface layer, more energy is released than in the 13–35 km layer, which indicates the predominant crustal position of chambers formed by highly productive magmatism. The exception is a single peak moment in the Iceland region, located northward to 67° N, which indicates a complex deep configuration of heated plume material. The main zones of seismicity maxima separate the Northern and Southern hemispheres, as well as the transition from the Atlantic to the Arctic (Fig. 8, profile *2*). They differ in energy release in events with a shear mechanism [2]. The arctic transition has extrema in all intervals, which indicates deep disjunctive faults. The equatorial transition is not marked by events deeper than 35 km, but the moment values at the two upper intervals are synchronized. However, the northern part of this transition near the Sierra Leone and Vema fracture zones has extrema only in the crustal interval, which appears unusual when compared with the southern frame of the equatorial transition.

In the spatiotemporal mapping along the MAR, zones of the strongest and most stable seismicity in time, conditionally called bands, and zones of their stable absence, called voids, are distinguished (Fig. 8, profile *3*). The bands in plan view, as well as other geological and geophysical parameters, correspond to the largest lateral displacements of the MAR axis along the transform faults (Fig. 1):

— Chain–Romanche–São Paulo group (from 1.5° S to 1.5° N);

— Arkhangelsky–Doldrums–Vernadsky group (from 7° N to 9° N);

— Vema fracture zone (11° N);

— dual Charlie–Gibbs fracture system (52° N);

— the fragment of the Mohns Ridge adjoining the Knipovich Ridge from the south (from 71° N to 74° N).

These zones are known for predominant of chamber shear mechanisms and do not reflect a magmatic along-axis process, with the exception of the eastern part of the Mohns Ridge, which is an exception in the observed pattern [2] (Fig. 8, profile *3*). The seismic tomography section along the MAR shows that in the area of these shear zones, the cold mantle is the shallowest position, responsible for an increased degree of fracturing between areas with contrasting properties (Fig. 8, profile *4*). The transition from the Mohns to the Knipovich Ridge is characterized by a discontinuity in the depth of the cold region, which probably creates the contrast in rheological properties responsible for the increased seismicity.

Another important feature of the spatiotemporal distribution is the presence of seismicity voids. If we consider the most obvious cases—from 10° S. up to 8° S (Ascension Island segment and segments in the Azores and Icelandic plumes—it becomes clear that the voids reflect zones of high-productivity magmatism (Fig. 8, profile *3*). According to the tomography data of different models, voids along the MAR correspond nearly everywhere to the strongest negative anomalies, which indicates low-viscosity zones within a single along-axial negative velocity anomaly (Fig. 7, profile *5*; Fig. 8, profile *4*). The absence in the voids of teleseismic events with a high detection threshold does not indicate absence of seismicity. The absence of conditions for accumulation of large stresses and large-magnitude seismic events was revealed.

CONCLUSIONS

(1) Thermal mantle inhomogeneities of fixed size, depicted as variations in seismic wave velocities, look larger than their true sizes in low-detail tomographic models. An increase in the detail of models shows how the heated and partially melted mantle regions actually look in the velocity variation field, which earlier, when analyzed using low-resolution models, merged into a single deep (up to 700 km) negative δV_s anomaly along the axis of the MAR; according to the theory, this should be due to general mantle convection. The depicted depth of the axial anomaly was gradually corrected up to 120 km as the detail was increased, which is shown by comparison with models having different levels of detail.

(2) An increase in the detail of tomographic models confirms the conclusion about the presence of two different types of upwelling in the mantle under the MAR axis and in the branches of superplumes: active-plume and passive-axial, which does not have deep roots and most likely arose as a response to the formation of space as lithospheric plates diverged. According to modern models, continuous anomalies from the surface to the boundary with the core, associated with ascending zones along the divergent boundaries of convective cells, have not been detected in the mantle. Anomalies of negative sign under the MAR are not observed deeper than 300 km in the models of the late 1990s and early 2000s. Modern models show the depth of a hot anomaly under the MAR up to 120 km, which is closer to the solidus depth. The symmetrical loca-

tion of local minima within the branches of superplumes shows that the intensity of the ascent of heated matter is impulsive, which is nearly synchronous for other branches of superplumes throughout the mantle.

(3) Comparison of seismic velocity anomalies with variations in the gravity field on the surface shows that their low-frequency components coincide with the minima of the seismic tomographic section represented by zones of decompacted mantle. Areas with heated and decompressed material in Bouguer anomalies are depicted by minima, which are the deeper, the deeper the roots of the anomalous zones in the mantle. The productivity of magmatism in these zones is especially high, and the relief formed by basalt eruptions has an elevated level and is depicted in anomalies in free air by maxima. The geophysical characteristics of the gravity field at the level of extended (>500 km) anomalous zones of the section have an antiphase behavior and a consistent physically substantiated interpretation due to the rheological state of the mantle, revealed by tomography data.

(4) Comparison of the petrological characteristics of basalts dredged along the MAR and tomography data shows that the velocity models of the upper mantle with the modern level of detail can already serve as a basis for comparison with geochemical characteristics and their prediction in areas without sampling of oceanic basement rocks.

(5) The desintegration of a single axial tomographic anomaly under the Mid-Atlantic Ridge into a chain of vertical lenses under slow spreading conditions corresponds to geochemical data on the discrete occurrence along the Mid-Atlantic Ridge of basalts of different associations with different depths of melt separation, which mix during fast spreading.

(6) The section of the attribute $\delta(V_p/V_s)$ along the MAR in the mantle above ~700 km contains cold lenses with a thickness of 200–300 km, which are spatially related to the following structural and tectonic phenomena:

— in the area of the Romanche and Charlie–Gibbs faults and the zone of the Knipovich Ridge, located above cold lenses, the maximum sublatitudinal displacement of the MAR axis with a left-lateral strike-slip morphology is observed;

— geochemical segmentation of the MAR and variations in the petrological parameters of basalts correlate well with areas of the cold mantle;

— modulation of the total lengths of transform faults, including passive parts, with increased values above cold lenses with an average step of spatial pulsations of this parameter of about 12° (1320 km). It is comparable with the depths of manifestations of cold blocks in the upper mantle;

— the asymmetry of spreading half-velocities is reduced to almost zero on the segments of the MAR, which are located above the cold lenses and near the maxima of modulation of the lengths of transform faults;

— between cold lenses, the half-rates spreading asymmetry reaches its maximum values. The negative correlation of half-rates maxima on the western and eastern flanks with a stable average along the isochrons means that the total spreading crustal buildup remains stable along the MAR;

(7) Cold mantle lenses at an average depth of ~500 km and the corresponding lithospheric characteristics are the background state, while the areas above hot segments are faults that occur in the places of plume branches. Taking into account the nature of the structure of the crust and upper mantle, divided into blocks by transform faults, inhomogeneous spreading rates can lead to displacements of blocks within large plates and various tectonic deformations of the intraplate space, as well as to conditions for differentiated horizontal displacement of masses with different and independent of each other kinematic characteristics. The fault network is formed in areas above cold blocks adjacent to hot and more mobile blocks.

(8) Along the 4 Ma isochron in the Northern Hemisphere, the spreading half-rates on the eastern flank of the MAR exceed those on the western. In the Southern Hemisphere, conversely, the spreading half-rates on the western flank exceed those on the eastern. The opposite value of the general asymmetry of spreading half-rates along the MAR in the Northern and Southern hemispheres may indicate effects of the Earth's rotation on the course of geodynamic processes along the axial structure of the Atlantic.

(9) Comparison of the half-rates profiles on the western and eastern flanks of the MAR shows that, against the general trend, there are local zones of inversion from the western predominance of increased velocities to the eastern one and, vice versa, in the Northern and Southern hemispheres. These spatial inversions are located in both hemispheres at approximately the same latitudes: between 20° and 25° and around 50° and 55°. Obviously, the position of these reversals indicates unstable zones, the dynamics in which is associated with rotational processes and zones of low mantle viscosity, which increase instability.

(10) The main demarcation zones—the equatorial zone and the transition from the North Atlantic to the Arctic—are characterized by maximum energy release with shear events and, according to seismic tomography data, are located near cold mantle lenses and a contrasting lateral transition to hot areas. The distribution of the total moment in the depth intervals 0–13 and 13–35 km is practically synchronous. The extrema of the plume branches of Bouvet, Tristan da Cunha, the Azores, and Iceland are represented by a larger moment in the surface layer, which indicates a predominantly crustal position of chambers associated with highly productive plume magmatism. Seis-

micity along the main space of the MAR, associated with standard basaltic magmatism, has a background character and does not make a significant contribution to the overall picture compared to shear zones.

(11) Stable areas of intense seismicity in spatiotemporal mapping along the MAR correspond to fault zones, primarily, to demarcation transform faults with a large lateral displacement of the MAR, also located, according to seismic tomography data, above cold mantle lenses. Stable regions of less intense seismicity are located in areas where the MAR intersects with plume branches.

ACKNOWLEDGMENTS

The authors are grateful to reviewers Prof. E.P. Dubinin (Moscow State University, Moscow, Russia) and Dr. A.A. Peyve (GIN RAS, Moscow, Russia) for comments that allowed us to improve the article, as well as to the editor M.N. Shupletsova (GIN RAS, Moscow, Russia) for thorough editing and preparation of the article.

FUNDING

The study was funded by the Russian Foundation for Basic Research (project no. 20-15-50123).

CONFLICT OF INTEREST

The authors declare that they have no conflicts of interest.

OPEN ACCESS

REFERENCES

1. A. S. Alekseev, M. M. Lavrent'ev, V. G. Romanov, and R. G. Mukhometov, "A numerical method for determining the structure of the Earth's upper mantle," in *Mathematical Problems of Geophysics*, Ed. by M. M. Lavrent'ev and A. S. Alekseev (Vych. Tsentr Sib. Otd. Akad. Nauk SSSR, Novosibirsk, 1969), Vol. 2, pp. 143–165 [in Russian].
2. S. A. Boldyrev, *Seismogeodynamics of the Mid-Atlantic Ridge* (MGK, Moscow, 1998) [in Russian].
3. E. Bonatti, "Origin of the large fracture zones offsetting the Mid-Atlantic Ridge," Geotectonics **30** (6), 430–440 (1996).
4. L. V. Dmitriev, S. Yu. Sokolov, V. G. Melson, and T. O'Hirn, "The plume and spreading associations of basalt and their reflection in the petrological and geophysical parameters of the northern Mid-Atlantic Ridge," Russ. J. Earth Sci. **1** (6), 457–476 (1999).
5. L. V. Dmitriev and S. Yu. Sokolov, "Geodynamics of three contrasting types of oceanic magmatism and their reflection in the data of seismic tomography," Petrology **11** (6), 597–613 (2003).
6. L. V. Dmitriev, S. Yu. Sokolov, and A. A. Plechova, "Statistical assessment of variations in the compositional and $P-T$ parameters of the evolution of mid-oceanic ridge basalts and their regional distribution," Petrology **14** (3), 209–229 (2006).
7. N. L. Dobretsov, A. G. Kirdyashkin, and A. A. Kirdyashkin, *Deep Geodynamics* (GEO, Novosibirsk, 2001) [in Russian].
8. D. Zhao, F. Pirajno, and L. Liu, "Structure and dynamics of the mantle beneath Eastern Russia and adjacent regions," Russ. Geol. Geophys. **51** (9), 925–938 (2010).
9. A. V. Kotlyarov, V. Yu. Kolobov, V. A. Simonov, and A. V. Yakovlev, "Features of deep structure of the upper mantle beneath the Mid-Atlantic Ridge," in *Proceedings of the LII Tectonic Conference "Fundamental Problems of Tectonics and Geodynamics* (GEOS, Moscow, 2020), Vol. 1, pp. 340–344.
10. B. L. Lichkov, *To the Fundamentals of the Modern Theory of the Earth* (Leningrad. Gos. Univ., Leningrad, 1965) [in Russian].
11. L. I. Lobkovsky, A. M. Nikishin, and V. E. Khain, *The Modern Problems of Geotectonics and Geodynamics*, Ed. by V. E. Khain (Nauchn. Mir, Moscow, 2004) [in Russian].
12. A. O. Mazarovich, *Geological Structure of the Central Atlantic: Faults, Volcanic Edifices, and Ocean Floor Deformations* (Nauchn. Mir, Moscow, 2000) [in Russian].
13. S. P. Mashchenkov, E. M. Litvinov, A. G. Gorshkov, and I. P. Lukashevich, "Geophysical criteria of distinguishing the regional settings, favorable for the formation of deep polymetallic sulfides," in *Deep Structure and Geodynamics of Lithosphere of the Atlantic and Pacific Oceans*, Ed. by I. S. Gramberg and P. A. Stroev (Nauka, Moscow, 1992), pp. 151–178 [in Russian].
14. A. V. Nikolaev, A. S. Alekseev, G. M. Tsibul'chik, V. N. Troyan, G. A. Ryzhikov, T. B. Yanovskaya, and M. B. Surnev, *Problems of Geotomography* (Nauka, Moscow, 1997) [in Russian].
15. N. S. Sokolov, "Correlation of the geological and geophysical parameters along the axis of the Mid-Atlantic Ridge and pre-Arc settings on its eastern flank," Moscow Univ. Geol. Bull. **62** (6), 404–409 (2007).
16. S. Yu. Sokolov, "Tectonic peculiarities of the Mid-Atlantic Ridge based on the data on correlation between surface parameters and geodynamic state of the upper

mantle," Vestn. KRAUNTs. Nauki Zemle **32** (4), 88–105 (2016).

17. S. Yu. Sokolov, "Correlation of ages of intraplate magmatism of the Atlantic with magnetic ages and seismotomography data," in *Proceedings of the LII Tectonic Conference "Fundamental Problems of Tectonics and Geodynamics"* (GEOS, Moscow, 2020), Vol. 2, pp. 303–307.
18. T. Yu. Tveritinova, "Wave tectonics of the Earth," Geodynam. Tectonophys. **1** (3), 297–312 (2010). https://doi.org/10.5800/GT-2010-1-3-0023
19. V. G. Trifonov and S. Yu. Sokolov, "Towards the postplate tectonics," Herald Russ. Acad. Sci. **85** (7), 605–615 (2015).
20. V. G. Trifonov and S. Yu. Sokolov, "Sublithospheric flows in the mantle," Geotectonics **51**, 535–548 (2017). https://doi.org/10.7868/S0016853X1706008X
21. D. L. Anderson, T. Tanimoto, and Y. Zhang, "Plate tectonics and hotspots: The third dimension," Science **256**, 1645–1651 (1992).
22. ANSS Earthquake Composite Catalog (Historical), 2012. https://ncedc.org/anss/catalog-search.html. Accessed December 31, 2012.
23. T. W. Becker and L. Boschi, "A comparison of tomographic and geodynamic mantle models," Geochem., Geophys., Geosyst., **3**, 1–48 (2002). https://doi.org/10.1029/2000GC000168
24. M. Cannat, A. Briais, C. Deplus, J. Escarti, J. Georgen, J. Lin, S. Mercouriev, C. Meyzen, M. Müller, G. Pouliquen, A. Rabain, and P. da Silva, "Mid-Atlantic Ridge–Azores hotspot interactions: Along-axis migration of a hotspot-derived event of enhanced magmatism 10 to 4 Ma ago," Earth Planet. Sci. Lett. **173** (3), 257–269 (1999).
25. N. Coltice, L. Husson, C. Faccenna, and M. Arnould, "What drives tectonic plates?" Science Advances **5** (10), 1–9 (2019). https://doi.org/10.1126/sciadv.aax4295
26. V. Courtillot, A. Davaille, J. Besse, and J. Stock, "Three distinct types of hotspots in the Earth's mantle," Earth Planet. Sci. Lett. **167** (205), 295–308 (2003).
27. S. P. Grand, R. D. Van Der Hilst, and S. Widiyantoro, "Global seismic tomography: A snapshot of convection in the Earth," GSA Today **7** (4), 1–7 (1997).
28. L. V. Danyushevsky, "The effect of small amount of H_2O crystallization of mid-ocean ridge and backarc basin magmas," J. Volcanol. Geotherm. Res. **110**, 265–280 (2001).
29. L. V. Dmitriev, S. Yu. Sokolov, and N. S. Sokolov, "Migration of the Azores superplume: geophysical and petrologic evidence," Russ. J. Earth Sci. **3** (6), 395–404 (2001).
30. A. M. Dziewonsky, B. H. Hager, and R. J. O' Connel, "Large scale heterogeneities in lower mantle," J. Geophys. Res. **82**, 239–255 (1977).
31. A. M. Dziewonsky and J. Woodhouse, "Global images of the Earth's Interior," Science **236**, 37–488 (1987). https://doi.org/10.1126/science.236.4797.37
32. A. M. Dziewonski and D. L. Anderson, "Preliminary Earth Model (PREM)," Phys. Earth Planet. Inter. **25**, 297–356 (1981).
33. A. M. Dziewonski, F. Alessandro, W. Su, and R. Woodward, "Seismic tomography and geodynamics," AGU Geophys. Monogr. Ser. **76**, 67–105 (1993). https://doi.org/10.1029/GM076p0067
34. GPS Time Series Data, 2008. http://sideshow.jpl.nasa.gov/mbh/series.html. Accessed August 31, 2008.
35. S. P. Grand, R. D. van der Hilst, and S. Widiyantoro, "Global seismic Tomography: A snapshot of convection in the Earth," GSA Today **7** (4), 1–7 (1997).
36. K. Hosseini, K. J. Matthews, K. Sigloch, G. E. Shephard, M. Domeier, and M. Tsekhmistrenko, "SubMachine: Web-Based tools for exploring seismic tomography and other models of Earth's deep interior," Geochem., Geophys., Geosyst. **19** (5), 1464–1483 (2018). https://doi.org/10.1029/2018GC007431
37. M. K. Kaban, P. Schwintzer, I. Artemieva, and W. D. Mooney, "Density of continental roots: Compositional and thermal effects," Earth Planet. Sci. Lett. **209** (1), 53–69 (2003).
38. P. Koelemeijer, J. Ritsema, A. Deuss, and H.-J. van Heijst, "SP12RTS: A degree-12 model of shear- and compressional-wave velocity for Earth's mantle," Geophys. J. Int. **204**, 1024–1039 (2016). https://doi.org/10.1093/gji/ggv481
39. I. Yu. Koulakov and S. V. Sobolev, "A tomographic image of Indian lithosphere break-off beneath the Pamir Hindukush Region," Geophys. J. Int. **164**, 425–440 (2006). https://doi.org/10.1111/j.1365-246X.2005.02841.x
40. S. Lebedev and R. D. Van Der Hilst, "Global upper-mantle tomography with the automated multimode inversion of surface and S-wave forms," Geophys. J. Int. **173** (2), 505–518 (2008).
41. C. Li, R. D. Van Der Hilst, E. R. Engdahl, and S. Burdick, "A new global model for *P* wave speed variations in Earth's mantle," Geochem., Geophys., Geosyst. **9** (5), 1–21 (2008).
42. A. O. Mazarovich and S. Yu. Sokolov, "Hydrothermal fields in the Mid-Atlantic ridge: Setting and prospects for further discoveries," Russ. J. Earth Sci. **4** (6), 423–431 (2002).
43. R. D. Müller, M. Sdrolias, C. Gaina, and W. R. Roest, "Age, spreading rates, and spreading asymmetry of the world's ocean crust," Geochem., Geophys., Geosyst. **9** (4), 1–19 (2008). https://doi.org/10.1029/2007GC001743
44. L. S. Resovsky and M. H. Ritzwoller, "A degree 8 mantle shear velocity model from normal mode observations below 3 mHz," J. Geophys. Res. **104** (B1), 993–1014 (1999).
45. J. Ritsema, H. J. van Heijst, and J. Woodhouse, "Complex shear wave velocity structure imaged beneath Africa and Iceland," Science **286**, 1925–1928 (2000). https://doi.org/10.1126/science.286.5446.1925
46. D. T. Sandwell and W. H. F. Smith, "Marine gravity anomaly from Geosat and ERS-1 satellite altymetry,"

J. Geophys. Res. **102** (B5), 10039–10054 (1997). https://doi.org/10.1029/96JB03223

47. A. J. Schaeffer and S. Lebedev, "Global shear speed structure of the upper mantle and transition zone," Geophys. J. Int. **194** (4), 417–449 (2013).
48. W. Su and A. Dziewonski, "Predominance of long-wavelength heterogeneity in the mantle," Nature **352**, 121–126 (1991). https://doi.org/10.1038/352121a0
49. W. J. Su, R. L. Woodward, and A. M. Dziewonski, "Deep origin of mid-ocean-ridge seismic velocity anomalies," Nature **360**, 149–152 (1992). https://doi.org/10.1038/360149a0
50. W. J. Su, R. L. Woodward, and A. M. Dziewonski, "Degree 12 model of shear velocity heterogeneity in the mantle," J. Geophys. Res. **99** (B4), 6945–6980 (1994).
51. B. M. Urann, H. J. B. Dick, R. Parnell-Turner, and J. F. Casey, "Recycled arc mantle recovered from the Mid-Atlantic Ridge," Nat. Commun. **11**, 1–9 (2020). https://doi.org/10.1038/s41467-020-17604-8
52. USGS Earthquake Composite Catalog, 2019. https://earthquake.usgs.gov/earthquakes/search/. Accessed February 16, 2019.
53. R. D. Van der Hilst, S. Widiyantoro, and E. R. Engdahl, "Evidence of deep mantle circulation from global tomography," Nature **386** (6625), 578–584 (1997).
54. Y. S. Zhang and T. Tanimoto, "Ridges, hotspots and their interaction, as observed in seismic velocity maps," Nature **355** (6355), 45–49 (1992).